Exploring the Role of a Smartphone as a Motion Sensing and Control Device in the Wireless Networked Control of a Motor Test-bed

Jared A. Frank, Anthony Brill, Jonghyun Bae and Vikram Kapila
Mechanical and Aerospace Engineering, NYU Polytechnic School of Engineering, Brooklyn, NY, 11201, U.S.A.
{*jared.alan, brill.anthony, jhb454, vkapila*}*@nyu.edu*

Keywords: Attitude Sensing, Motor Control, Networked Control System, Smartphone Sensors, Wireless.

Abstract: The sensing, computing, and control potential of smartphones remains to be fully explored in automatic control applications. In this paper, we control the angular position of a motor test-bed using feedback from the embedded motion sensors of a smartphone while it is mounted to the test-bed. The smartphone hosts an interactive user interface which students and researchers can use to quickly and easily perform experiments with the test-bed and collect measurements using their own personal devices. Proportional-plus-derivative (PD) controllers designed using a sampled-data model of the system are compared for different sampling rates used on the smartphone. Results from simulations and experiments confirm the feasibility of utilizing mounted smartphones in the wireless networked control of systems with rotational degrees of freedom.

1 INTRODUCTION

Smartphones are more powerful than ever; embedded sensors, open and programmable architecture, and support for several communication protocols endow them with the potential to serve as lightwight, portable, inexpensive platforms for sensing in a wide array of applications (Lane, 2010). Several mobile applications have been developed that utilize the embedded sensors of smartphones for real-time monitoring. Some of the most popular of these sensors are the motion sensors, including accelerometer, gyroscope, and magnetometer. Algorithms for processing and integrating data from these sensors yield device attitude measurements accurate enough for clinical use in measuring the Cobb angle in both kyphoses (Jacquot, 2012) and scoliosis (Shaw, 2012). The motion sensors in smartphones have also been used for positioning applications in indoor environments where GPS signal is weak (Schindhelm et al., 2011) and to encourage autonomous navigation for visually impaired people (Moder et al., 2014). By analyzing accelerometer data, mobile applications can be used for activity recognition, e.g., to detect when users are walking, jogging, and ascending or descending stairs (Khan, 2010). The medical applications include use of smartphone accelerometer data to analyze gait characteristics (LeMoyne, 2010a), characterize Parkinson's disease tremor (LeMoyne, 2010b), and notify emergency services if a user has fallen (He et al., 2012).

Exploiting the sensing power of smartphones has led to improvements in feasibility and reductions in complexity in diverse applications. An artificial pancreas system has been developed that uses a smartphone to process wireless data from a continuous glucose monitoring (CGM) system worn by patients with type 1 diabetes (Kovatchev, 2013). Previous implementations consisted of the CGM and insulin pump wired to computers, which limited free movement and outdoor usage. A smartphone implementation may also yield cost reductions *vis-a-vis* conventional hardware. For instance, a system that processes accelerometer data from a smartphone to detect potholes has been proposed as a substitute for high-cost equipment (Mednis, 2011).

Although the incorporation of smartphones to monitor and interact with physical systems is now being investigated (Frank and Kapila, 2014), the potential role of these devices in the automatic, closed-loop networked control of systems remains largely unexplored. Notable exceptions include the construction of smartphone-controlled robots and unmanned vehicles. Although traditionally microprocessors onboard the vehicle are used to execute the robot's control algorithms, smartphones contain processors with multiple cores, real-time operating systems, and sufficient speed and memory to handle large computational loads (Aroca, 2012). Thus, smartphones have recently been used as navigation and guidance units for marine and aerial vehicles (El-Gaaly, 2013; Desai,

2013). In this role, the smartphone can use embedded sensors to detect obstacles in the environment, sense collisions, and estimate the pose of the robot as the processor computes vehicle velocities.

In this paper, we investigate the use of a smartphone as a wireless mountable motion sensing and control device in the automatic control of a motor test-bed. This implementation reduces the wiring, cost, and complexity involved in installing industrial-grade sensors and enables users to leverage the sensing, computation, and communication power of their mobile devices to quickly and easily drive simple single degree-of-freedom systems. Students and researchers in engineering laboratories can attach their own personal devices to the test-bed to automatically control it and collect data. An interactive user interface to the test-bed on the smartphone screen allows users to set parameters, such as control gains and set points for the system, and to save and email themselves the collected data for post-processing. An overview of the system is provided, including the motion sensing capability of the smartphone and the design of a 3D-printed mount for attaching the smartphone to the test-bed. PD controllers, which are to be implemented on the smartphone, are designed for several different sampling rates using a sampled-data model of the system. The motor's response to these controllers are explored in simulations and experiments. Since the accuracy, drift, and calibration of sensor data, as well as time delays associated with computation and wireless communication, can significantly impact the stability and performance of the system, the effects of these factors are measured and discussed in the context of the proposed system.

2 SYSTEM DESCRIPTION

The test-bed used in this study consists of a geared DC-motor attached to a power amplifier (see Figure 1). An incremental optical encoder and a multi-turn potentiometer are available to monitor the motor orientation and a tachometer is available to measure its angular rate. A desktop computer equipped with a PC-based data acquisition and control (DAC) board is used to transmit control signals to the power amplifier that drives the motor.

2.1 Mount Design

To secure the smartphone to the test-bed so that accurate orientation data is obtained from the motion sensors of the smartphone, a mount is designed and 3D-printed using polylactide (PLA) material (see Figure 2(a)). Using guidelines and dimensions provided by the smartphone manufacturer, the mount is designed with four tabs to clip the phone in place and prevent it from rotating with respect to the motor arm (see Figure 2(b)). The mount is designed to align the axis of rotation through the geometric center of the smartphone. Consideration is taken to not block the buttons or the screen of the smartphone so that a user interface may be used to interact with the test-bed.

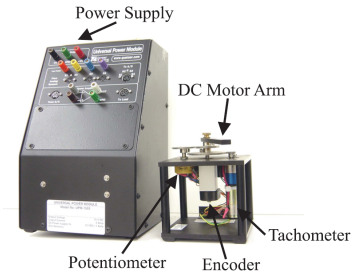

Figure 1: The motor test-bed used in this study.

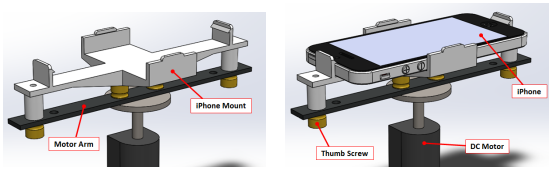

(a) (b)

Figure 2: Phone mount design (a) without and (b) with an iPhone 5 secured in between its tabs.

2.2 Embedded Sensing and Calibration

The smartphone used in this study is an Apple iPhone 5, which contains a three-axis accelerometer and gyroscope from STMicroelectronics and a magnetometer from AKM Semiconductor. Data from the first two sensors is used to estimate the attitude of the device. A single class is used for central access to raw data from each axis of the motion sensors. Estimates of device attitude and rotation rate are generated after processing raw data with sensor fusion algorithms. Device attitude is expressed in Euler angle form and defined as the rotation between the device's current reference frame and the initial reference frame that is established when the mobile application ("app") first begins collecting motion updates. In this study, the iPhone is rigidly mounted to the motor arm, which lies in the horizontal plane. Therefore, only data associated with the axis normal to the device screen is needed to estimate the orientation of the motor arm.

To obtain motion data, the app periodically samples the most recently available measurement at a specified rate known as the update interval. Choosing an update interval is an important part of the design of the system since it has a significant impact on

the performance of the closed-loop. This interval is referred to as the sampling rate in the sampled-data model that characterizes the closed-loop behavior of the wireless networked control system. With a larger update interval, the embedded sensors are polled less often by the app, improving battery consumption. While 10-20 Hz sampling frequency may be suitable for many teleoperation tasks, Apple's event handling guidelines recommend a range of 30-60 Hz for collecting device orientation data for real-time applications. Mobile applications developed for iOS support update frequencies up to 100 Hz for detecting high-frequency motions, such as impacts and quick shakes. After performing an experiment involving the collection of 350 samples, the mean motion data computation time on the smartphone is determined to be 244.4 microseconds with a standard deviation of 91.168 microseconds. This gives a 95% confidence interval of $[239.13, 258.36]$ microseconds for the mean, which is fast enough to support a 100Hz sampling rate.

Calibration of the embedded sensors is performed using the potentiometer sensor on the test-bed. Experiments are initiated at the orientation in which the potentiometer outputs zero volts. Therefore, the angular position readings from the smartphone and the potentiometer are aligned. However, experiments show that the readings of device attitude drift over time with respect to readings from the potentiometer (see Section 5.1). In future work, the use of the embedded magnetometers of smartphones will be investigated to both calibrate the system and improve the accuracy of readings by correcting against drift.

2.3 Communication

Wireless communication of data between the smartphone and the desktop computer is performed using a traditional client-server architecture, with a server running on the desktop computer and the client running on the smartphone app. Data is sent and received using the TCP/IP protocol over a wireless local area network, which is maintained by a Wi-Fi router. The Nagle algorithm, a standard method of improving the efficiency of the network, is built into the TCP/IP protocol. This algorithm combines small outgoing messages that cause a sufficiently large overhead and sends them all at once in a burst (Nagle, 1995). This process introduces latency, so the Nagle algorithm is disabled on both sides of the communication to allow data to be sent and received in real-time.

To test communication on the wireless network, a command is issued on the desktop computer to ping the smartphone and another computer. After sending 100 echo requests with 32 byte packets, the average round trip times for the smartphone and the other computer are determined to be 78.11 ms and 30.79 ms, respectively. A paired t-test is conducted to test whether the two sets come from distributions with equal means. With a 95% confidence level, the null hypothesis could be rejected (with $t(99) = 2.324$, $p = 0.022 < 0.05$, $95\%CI = [6.927, 87.713]$). Thus, the communication with the smartphone experiences larger latency than a typical desktop computer on the same network.

Network latency results in time delays between data collected by the sensors on the test-bed and the embedded sensors of the smartphone. These time delays in the closed-loop system can vary significantly, which can cause degradation in system stability and performance and complicate analysis and control design. Several control methodologies have been used over the last several decades to compensate for such effects, spanning the use of Smith predictors, optimal stochastic methods, fuzzy logic, and queuing and buffering. However, with a mean one-way communication delay of 39.055 ms, average delays in the system are only between 0 and 4 sampling periods, depending on the sampling rate used. As will be shown in Section 5.2, this amount of delay is negligible when controlling the motor test-bed, whose bandwidth is sufficiently low.

3 USER INTERFACE DESIGN

Mounting the smartphone to the test-bed can add portable sensing, computing, and control capability to the system, as well as provide an interactive user interface attached to the motor arm. Figure 3shows screenshots of a mobile app implemented on an iPhone 5 device, allowing users to start and stop experiments as well as issue reference commands from the smartphone touch screen. A connect button on the interface establishes wireless communication with the compu-

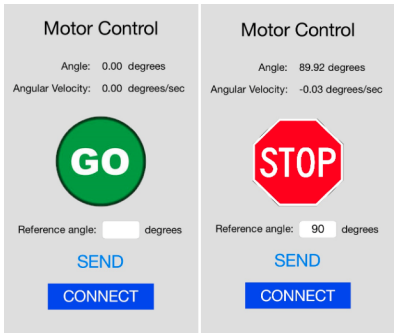

Figure 3: Screenshots of the mobile application's user interface on an iPhone 5.

ter, and a text field is used to issue a reference angle for position control. Sensor data is displayed in real-time on the screen using text labels. A button to start and stop the experiment is located in the center of the screen so that the position of the button is not affected by the rotation of the device, making it easy for users to stop the motor in case of an emergency while the experiment is running.

4 MODELING AND CONTROL DESIGN

To control the orientation of the motor arm using a mounted smartphone, the mobile app on the smartphone computes the control action $u(t)$ at time $t = kT$, where T is the sampling rate and $k = 0, 1, 2, \ldots$, after the angle $\theta(kT)$ and angular rate $\omega(kT)$ have been sampled. This control computation is done according to the PD control structure

$$u[kT] = K_{\mathrm{p}}\theta[kT] + K_{\mathrm{d}}\omega[kT].$$

To design the proportional and derivative control gains K_{p} and K_{d}, respectively, the standard pole-placement technique is used in discrete-time. First, the continuous-time model of the plant is obtained. Next, the model of the plant is discretized to model the fixed-rate sampling of motion data and control computation by the smartphone. PD controllers are designed and compared for several sampling rates.

4.1 Plant Model

The plant, composed of an armature-controlled DC-motor, gearbox, and load (i.e., the motor arm, mount, and the smartphone), has a dynamic behavior that can be captured by a first-order transfer function from voltage input to the motor $V_{\mathrm{a}}(s)$ to the angular velocity of the motor $\Omega(s)$

$$\frac{\Omega(s)}{V_{\mathrm{a}}(s)} = \frac{K}{\tau s + 1},$$

where K is the steady-state gain and τ is the time-constant. A unit-step voltage is applied to the plant to experimentally identify the values of K and τ as 1.5981 Volts and 0.029 seconds, respectively.

4.2 Discretization

The effect of the smartphone in the loop, notably the discrete-time sampling of data, must be considered in the control design. A sampled-data model is used to describe the proposed system in which the smartphone performs the sensing and the control computation for the test-bed. Samplers and zero-order holds are introduced in the feedback paths and in the feed-forward path of the closed-loop (see Figure 4). These samplers represent the sampled attitude and angular velocity data handled by the smartphone, as well as the control action computed using the PD control algorithm running on the backend of the mobile app. Since the control data is transmitted to the host machine in the same TCP/IP packet as the sensor readings, which are used by the host machine only for data logging, the three samplers are assumed to share the same uniform sampling rate T.

In choosing the sampling rate on the smartphone such that the closed-loop system is stable, it is required that the sampling rate be sufficiently fast relative to the dynamics of the plant. A commonly used rule of thumb in digital control design is to keep the sampling rate faster than 30 times the closed-loop bandwidth frequency, ω_{b}, which is calculated directly from values of damping ratio ζ and natural frequency ω_n (Kuo, 1980)

$$\omega_b = \omega_n[(1-2\zeta^2) + \sqrt{4\zeta^4 - 4\zeta^2 + 2}]^{1/2}.$$

To design PD controllers such that the step response of the closed-loop system exhibits no overshoot and a settling time T_{s} of less than one second, the desired natural frequency ω_n and damping ratio ζ are obtained (Dorf and Bishop, 2007)

$$\zeta = 0.9959, \quad \omega_n = -\log(0.02)/(\zeta \times T_{\mathrm{s}}) = 3.9282.$$

Therefore the value of the bandwidth is calculated to be 2.5429 rad/sec (0.4047 Hz), which means that the sampling rate used with the smartphone should be larger than ≈ 12.2 Hz. To compare the system performance at various sampling rates supported by the smartphone processor, PD-controllers will be designed using a discretized state-space representation of the closed-loop system with sampling rates set to $1, 5, 10, 30, 60$, and 100 Hz. The open-loop transfer function for the plant can be transformed into a state-space representation in which the state is a vector of the angular orientation and rate, $x(t) \triangleq \begin{bmatrix} \theta(t) & \omega(t) \end{bmatrix}^{\mathrm{T}}$, yielding

$$\dot{x} = Ax + Bu, \quad y = Cx,$$

$$A \triangleq \begin{bmatrix} 0 & 1 \\ 0 & -\frac{1}{\tau} \end{bmatrix}, \quad B \triangleq \begin{bmatrix} 0 \\ \frac{K}{\tau} \end{bmatrix}, \quad C \triangleq \begin{bmatrix} 1 & 0 \end{bmatrix}.$$

This state-space representation can be discretized, at each sampling instant kT, $k = 0, 1, 2, \ldots$, as follows (Kuo, 1980)

$$x[(k+1)T] = \phi(T)x[kT] + \gamma(T)u[kT],$$
$$y[kT] = Cx[kT],$$

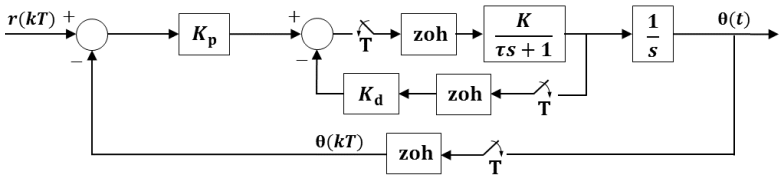

Figure 4: Sampled-data block diagram of the closed-loop system.

where $\phi(T) \triangleq e^{AT}$ is the state transition matrix of the state matrix A of the continuous-time state equation and $\gamma(T) \triangleq \int_0^T \phi(T-\tau)Bd\tau$. Before designing controllers, the controllability of this second-order system is verified by confirming that the 2×2 controllability matrix $M_c = \begin{bmatrix} \phi(T) & \phi(T)\gamma(T) \end{bmatrix}$ of the system has full rank. Indeed, the sampled-data models are found controllable and since the state vector contains the angular orientation and rate, the PD controllers can be designed with the digital full-state feedback control law $u[kT] = -K_c x[kT]$, where $K_c = \begin{bmatrix} K_p & K_d \end{bmatrix}^T$ is the PD-control gain matrix.

4.3 Controller Design

The continuous-time transfer function of the DC-motor controlled by a continuous-time PD controller $u(t) = k_p\theta(t) + k_d\omega(t)$ is

$$\frac{\Theta(s)}{R(s)} = \frac{\frac{Kk_p}{\tau}}{s^2 + \frac{(1+Kk_d)}{\tau}s + \frac{Kk_p}{\tau}},$$

where $R(s)$ and $\Theta(s)$ denote the reference command and angular position output, respectively. The prototype second-order transfer function is

$$\frac{Y(s)}{U(s)} = \frac{\omega_n^2}{s^2 + 2\zeta\omega_n s + \omega_n^2}.$$

Matching coefficients, the nominal expressions for the control gains are found

$$k_p = \frac{2\zeta\omega_n\tau - 1}{K}, \quad k_d = \frac{\omega_n^2\tau}{K}.$$

Plugging numerical values of K, τ, ζ, and ω_n gives $k_p = 0.2800$ and $k_d = -0.4838$. To design controllers based on discretized models of the plant using the pole-placement technique, the prototype second-order system is discretized. Then, the desired characteristic equation is determined in the z-domain from the discretized state-space matrix A_d

$$\lambda(z, A_d) = |zI - A_d|.$$

Using Ackermann's formula, the controller gain matrix $K_c(T)$ for the system discretized at a sampling rate T can be computed from the controllability matrices $M_c(T)$ and the matrix returned by plugging the discretized state matrix $\phi(T)$ into the desired characteristic equation (Dorf and Bishop, 2007)

$$K_c(T) = [0 \quad 1]M_c^{-1}(T)\lambda(z, \phi(T)).$$

Table 1: PD Control Design Parameters.

Sampling Rate	Open-Loop Poles	Desired Poles	Controller $[K_p, K_d]$
1 Hz	1, 0.0000	$0.0187 \pm 0.0070\imath$	[0.6025, 0.0172]
5 Hz	1, 0.0010	$0.4561 \pm 0.0325\imath$	[0.9296, -0.1036]
10 Hz	1, 0.0318	$0.6758 \pm 0.0241\imath$	[0.6830, -0.2574]
30 Hz	1, 0.3168	$0.8777 \pm 0.0104\imath$	[0.4141, -0.4099]
60 Hz	1, 0.5629	$0.9369 \pm 0.0056\imath$	[0.3450, -0.4481]
100 Hz	1, 0.7083	$0.9616 \pm 0.0034\imath$	[0.3184, -0.4628]

5 EXPERIMENTAL RESULTS

5.1 Sensor Noise and Accuracy

Drift errors associated with gyroscope-based orientation estimates have been observed and documented over the past decades (Oravetz and Sandberg, 1970). Commercially available devices have been found to provide reliable estimates of orientation when used for periods of up to one minute (Luinge and Veltink, 2005). Fortunately, the proposed system is expected to be stabilized within a few seconds. To investigate the noise and drift characteristics of the smartphone sensor data, two 20 second tests are conducted with the smartphone sensors (sampled at 60 Hz) and the potentiometer and tachometer sensors on the test-bed. The first test involved collecting sensor data while the motor is held at the zero orientation without being driven. The angular position data from the smartphone sensors and potentiometer sensor are shown in Figure 5(a) for this static test. Smartphone attitude data has an average drift rate of $1.0297x10^{-4}$ rad/sec (0.0059°/sec). Angular rotation rate data from the gyroscope and the tachometer are shown in Figure 5(b). Data from the tachometer has a slight bias; the mean of the gyroscope data is $-1.4439x10^{-4}$ rad/sec (−0.0083°/sec) while the tachometer mean is 0.0038 rad/sec (0.2177°/sec). However, the data from the smartphone is much noisier and causes drift

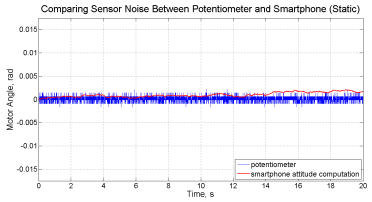

(a)

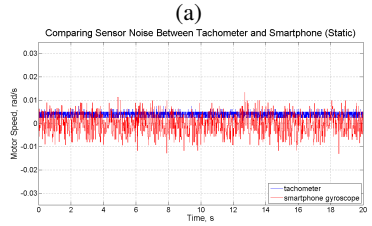

(b)

Figure 5: Comparisons between (a) the smartphone attitude sensing and potentiometer readings and (b) the smartphone gyroscope readings and tachometer readings while the motor is not being driven.

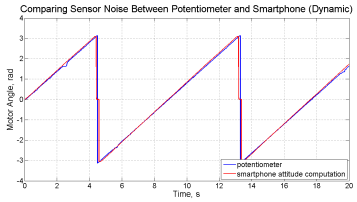

(a)

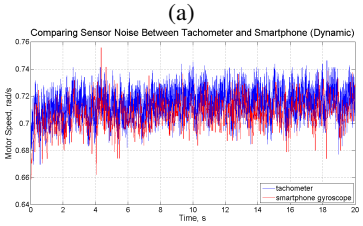

(b)

Figure 6: Comparisons between (a) the smartphone attitude sensing and potentiometer readings and (b) the smartphone gyroscope readings and tachometer readings while the motor is being driven by a 0.5 Volt signal.

in smartphone attitude. The standard deviation of the gyroscope is 0.0044 rad/sec (0.2521°/sec) compared to $7.0937x10^{-4}$ rad/sec (0.0406°/sec) for the tachometer.

The second test involved collecting sensor data while the motor is driven from its zero orientation with a constant 0.5 Volt signal. The angular position measurements from the smartphone and from the potentiometer of the test-bed are shown together in Figure 6(a). At the beginning of the run, the difference between the angular position readings is 0.0030 rad $(0.1719°)$ and at the end of the run, the difference is -0.0174 rad $(-0.9969°)$. Over the course of the run, the mean difference between the two sensors is -0.0247 rad $(-1.4152°)$. This represents a sufficiently small amount of error for the case when the motor is continuously driven over a long time interval. The measurements from the gyroscope of the smartphone and from the tachometer of the test-bed are shown together in Figure 6(b). The mean reading for the angular speed reported by the gyroscope is 0.7070 rad/sec $(40.5081°/\text{sec})$ compared to the tachometer's 0.7163 rad/sec $(41.0410°/\text{sec})$, indicating a difference of just 0.0093 rad/sec $(0.5329°/\text{sec})$. The standard deviation of the smartphone's gyroscope for this test is 0.0113 rad/sec $(0.6474°/\text{sec})$ and for the tachometer 0.0107 rad/sec $(0.6131°/\text{sec})$, showing that the two sensors have noise of a similar magnitude during this dynamic test.

To stabilize the motor test-bed, attitude estimates are only needed for a few seconds. Therefore, readings from embedded gyroscopes and accelerometers are sufficient to provide such estimates. For long-term use, additional sensors such as onboard three-axis magnetometers can provide additional sensory information necessary to eliminate drift. Traditional approaches of fusing the data between the three sensors make use of unscented Kalman filters (Harada, 2003), extended Kalman filters (Marins, 2001), and other filtering techniques. The implementation of such techniques using the embedded magnetometer on the smartphone will be explored in future work.

5.2 Controlling the Test-bed

To explore the feasibility of controlling the motor test-bed using the attitude and speed measurements collected by the smartphone and running the PD-control algorithm directly on the smartphone, trials are conducted in which the motor is given a step input command of 90° (1.5708 rad). Figures 7(a)–7(f) show the motor's closed-loop response at each sampling rate. By plotting the angular position data reported by the smartphone next to the readings of the potentiometer as it is sampled by the desktop computer at 1,000 Hz, one can visualize the communication delay between the smartphone and computer as well as the drift in the smartphone sensor data. Note that the results of simulation are also plotted alongside the experimental results. For comparison purposes, Figure 7(g) shows the response when the nominal PD controller is implemented on the desktop computer using feedback from the potentiometer and tachometer sensors of the test-bed.

Table 2 shows the values of the percent overshoot and settling time for each of the responses depicted in Figure 7. These results show that the percent overshoot and settling time increase as the sampling rate of the smartphone is decreased, indicating an improvement in the responsiveness of the closed-loop

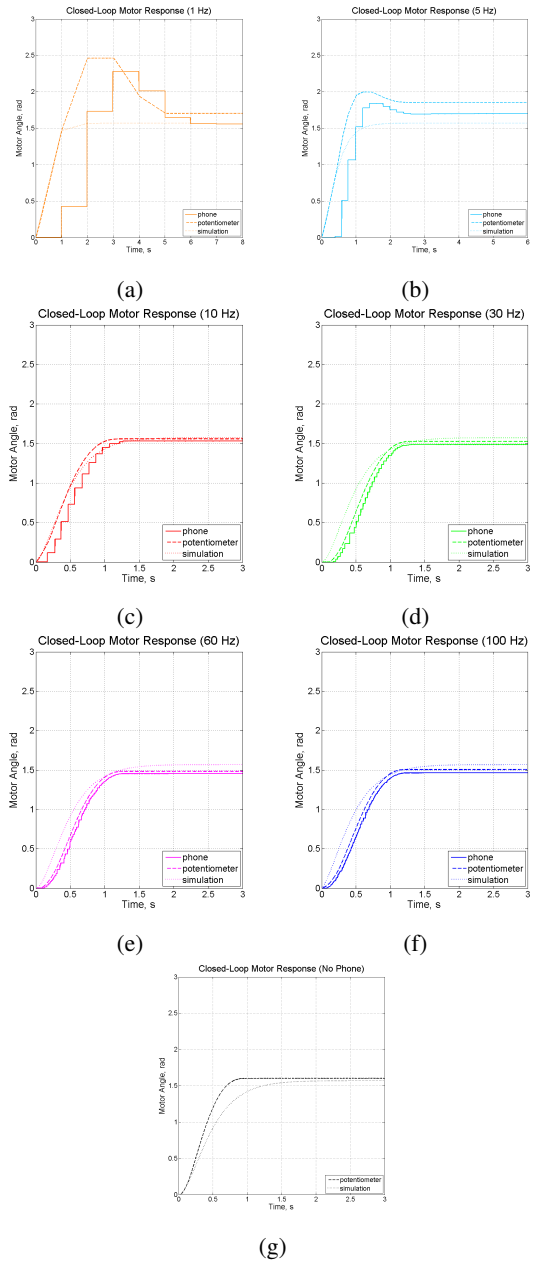

Figure 7: Closed-loop responses with the redesigned controller implemented using the smartphone (a–f) and the nominal controller implemented using the computer (g).

system as the sampling rate becomes faster. Note that a large deterioration in the quality of the performance is observed from the motor when the smartphone-based controller is run slower than 10 Hz. Since 5 Hz and 1 Hz are significantly less than 30 times the closed-loop bandwidth frequency, sampling the motor system at these rates leaves a large amount of inter-sample behavior uncaptured by the smartphone, causing a significant loss in performance. Finally, each response exhibits varying degrees of steady-state error, which can be attributed to mechanical properties of the motor and gearbox, such as friction, that result in a deadzone in the motor's sensitivity around 0 Volt. This steady-state error can be overcome with the introduction of an integral term to the controller. Note that by designing the controllers using the sampled-data model, the response of the motor at each sampling rate is more or less consistent and varies little from one sampling rate to another.

Table 2: Motor response performance using the digitally redesigned PD-control implementation.

Sampling Rate	Maximum Overshoot (%)	Settling Time (s)
no phone	0.00	0.798
100 Hz	0.00	1.096
60 Hz	0.00	1.128
30 Hz	0.00	1.140
10 Hz	0.00	1.216
5 Hz	8.12	2.188
1 Hz	46.23	5.986

To confirm that time delays introduced by the wireless network latency may be neglected in the design of the proposed system, a simulation of the sampled-data model was built in the MATLAB/Simulink environment with a constant delay of 39.055 ms introduced (the mean one-way communication time measured in Section 2.3). As can be seen in Figure 7, the experimental results match the simulated responses quite well, indicating that delays of 0-4 sampling periods are not significant when controlling a system with such a low bandwidth. In future work, the use of the proposed system with more time-sensitive, high-bandwidth plants will be explored.

With a low closed-loop bandwidth, a large range of sampling rates may be used to stabilize the proposed system. However, it is observed that the battery is consumed quicker at faster sampling rates, since the sensors as well as the communication module consume a substantial amount of a smartphone's power. Therefore, a sampled-data model can be used to design a controller to be implemented on the smartphone at a sampling rate just about 30 times the closed-loop bandwidth frequency.

6 CONCLUSIONS

This paper explored an approach to wirelessly control the orientation of a motor test-bed using feedback from the embedded motion sensors of a smartphone mounted to the test-bed. The study explored the case of performing the control algorithm on the smartphone itself. A PD control algorithm was used, with controllers running at several different sampling

rates being compared. Results from simulations and experiments validate the feasibility of using a smartphone to serve as the sensing and control platform in the automatic control of systems with a single rotational degree of freedom. Future work will consider extensions to more complex systems with both rotational and translational degrees of freedom, such as an inverted pendulum on cart system. Studies with students will be conducted to investigate whether the use of mobile devices in the proposed manner is engaging and provides access to more effective, interaction-based educational, training, and research experiences in the fields of automatic and digital control.

ACKNOWLEDGEMENTS

This work is supported in part by the National Science Foundation awards RET Site EEC-1132482, GK-12 Fellows DGE: 0741714, and DRK-12 DRL: 1417769, and NY Space Grant Consortium grant 48240-7887. The authors would like to thank Matthew Moorhead for the design and fabrication of the smartphone mount.

REFERENCES

Aroca, R.V., *et al*. (2012). Towards smarter robots with smartphones. In *5th Workshop in Applied Robotics and Automation*, pages 1–6.

Desai, A., *et al*. (2013). Stabilization and control of quad-rotor helicopter using a smartphone device. In *IS&T/SPIE Electronic Imaging*, page 866208.

Dorf, R. and Bishop, R. (2007). *Modern Control Systems (11th ed.)*. New Jersey: Prentice Hall.

El-Gaaly, T. *et al*. (2013). Visual obstacle avoidance for autonomous watercraft using smartphones. In *Autonomous Robots and Multirobot Systems Workshop*.

Frank, J. and Kapila, V. (2014). Development of mobile interfaces to interact with automatic control experiments [focus on education]. *IEEE Control Systems*, 34(5):78–98.

Harada, T., *et al*. (2003). Portable orientation estimation device based on accelerometers, magnetometers and gyroscope sensors for sensor network. In *IEEE Int. Conf. Multisensor Fusion and Integration for Intelligent Systems*, pages 191–196.

He, Y., Li, Y., and Yin, C. (2012). Falling-incident detection and alarm by smartphone with multimedia messaging service (MMS). *E-Health Telecommunication Systems and Networks*, 1(1):1–5.

Jacquot, F., *et al*. (2012). Measuring the Cobb angle with the iPhone in kyphoses: A reliability study. *International Orthopaedics*, 36(8):1655–1660.

Khan, A.M., *et al*. (2010). Human activity recognition via an accelerometer-enabled smartphone using kernel discriminant analysis. In *Int. Conf. Future Information Technology*, pages 1–6.

Kovatchev, B.P., *et al*. (2013). Feasibility of outpatient fully integrated closed-loop control first studies of wearable artificial pancreas. *Diabetes Care*, 36(7):1851–1858.

Kuo, B. (1980). *Digital Control Systems (2nd ed.)*. Oxford University Press.

Lane, N.D., *et al*. (2010). A survey of mobile phone sensing. *IEEE Communications Magazine*, 48(9):140–150.

LeMoyne, R., *et al*. (2010a). Implementation of an iPhone as a wireless accelerometer for quantifying gait characteristics. In *IEEE Int. Conf. Engineering in Medicine and Biology Society*, pages 3847–3851.

LeMoyne, R., *et al*. (2010b). Implementation of an iPhone for characterizing Parkinson's disease tremor through a wireless accelerometer application. In *IEEE Int. Conf. Engineering in Medicine and Biology Society*.

Luinge, H. and Veltink, P. (2005). Measuring orientation of human body segments using miniature gyroscopes and accelerometers. *Medical and Biological Engineering and Computing*, 43(2):273–282.

Marins, J.L., *et al*. (2001). An extended kalman filter for quaternion-based orientation estimation using MARG sensors. In *IEEE/RSJ Int. Conf. Intelligent Robots and Systems*, volume 4, pages 2003–2011.

Mednis, A., *et al*. (2011). Real time pothole detection using Android smartphones with accelerometers. In *Int. Conf. Distributed Computing in Sensor Systems and Workshops*, pages 1–6.

Moder, T., Hafner, P., and Wieser, M. (2014). Indoor positioning for visually impaired people based on smartphones. In *Computers Helping People with Special Needs*, pages 441–444.

Nagle, J. (1995). Congestion control in IP/TCP internetworks. *ACM SIGCOMM Computer Communication Review*, 25(1):61–65.

Oravetz, A. and Sandberg, H. (1970). Stationary and nonstationary characteristics of gyro drift rate. *AIAA Journal*, 8(10):1766–1772.

Schindhelm, C., Gschwandtner, F., and Banholzer, M. (2011). Usability of Apple iPhones for inertial navigation systems. In *IEEE Int. Symp. Personal Indoor and Mobile Radio Communications*, pages 1254–1258.

Shaw, M., *et al*. (2012). Use of the iPhone for Cobb angle measurement in scoliosis. *European Spine Journal*, 21(6):1062–1068.